

# Phase driven magnetic and optoelectronic properties of La<sub>2</sub>CrNiO<sub>6</sub>: A DFT and Monte Carlo perspective

Tushar Kanti Bhowmik\*, Tripurari Prasad Sinha

*Bose Institute, Department of Physics, 93/1, APC Road, Kolkata- 700009, India*

---

## Abstract

In search of the ferromagnetic insulators for spintronic device applications, we have studied the electronic, optical and magnetic properties of La<sub>2</sub>CrNiO<sub>6</sub> (LCNO) using the first principle density functional theory (DFT) and monte carlo simulation technique. Firstly, we have adopted the sol-gel method for preparation of LCNO and refined the X-ray diffracted value using the fullprof suite under the Rietveld mechanism. The obtained orthorhombic Pbnm and cubic Fm-3m space groups are used as the input of the DFT calculations. Both the structures have shown the half metallicity and insulating band gap towards the majority and minority spin direction respectively. From the magnetic moment calculations, we have seen the low spin state of Ni<sup>3+</sup> and the double exchange (DE) interaction is responsible for the ferromagnetism of LCNO. The optical dielectric constant is 10 and the refractive index is 3.2 for orthorhombic structure. The transition temperature ( $T_C$ ) is determined to 110 K from MCS study, which has well agreed with experimental value (111 K). The RCP value is determined to 12 J/Kg with a 5

---

\*Corresponding author

*Email address:* `physics.tushar@gmail.com` (Tushar Kanti Bhowmik )

tesla applied field, which is good for magnetocaloric applications.

*Keywords:* Magnetic properties, Ferromagnetic insulator, DFT, Monte Carlo simulation, Rietveld refinement, Double exchange, Half metallicity, RCP, Magnetocaloric effect

---

## 1. Introduction

Double perovskites ( $A_2B'B''O_6$ , where, A is larger cation, B' and B'' are smaller cations than A) have taken tremendous interest due to its versatile properties and applications. When the B- site is filled with 3d transition metals, it introduces various properties, such as different magnetic states [1–3], electron hopping conduction [4], ferromagnetic insulator [5–8], magnetodielectric [9], magnetocapacitance [10], magnetoresistance [11], large magnetocaloric effect [12] etc. Most of these properties arises due to the  $BO_6$  octahedra, where the B- site transition metal and oxygen transfers electron through the double exchange [13], super exchange mechanism [14]. Based on these properties, the double perovskites have been applied in storage devices [15], magnetic cooling technologies [12], spintronics [16, 17], opto-electronics [18], piezoelectrics [19] etc. For spintronics devices, a ferromagnetic insulator along with a non magnetic conductor restricts the electron transport through the non magnetic region. Some of the ferromagnetic insulators which belongs to the double perovskites are  $La_2NiMnO_6$  [5],  $La_2CoMnO_6$  [6],  $La_2CrNiO_6$  [20],  $Sr_2FeReO_6$  [21] etc. The underlying physics behind these FM insulator is very interesting due to their 3d and 5d orbitals. Again, the ferromagnetism always try to accompany the metallic behaviour in the materials. So, these two opposite nature alongside these materials

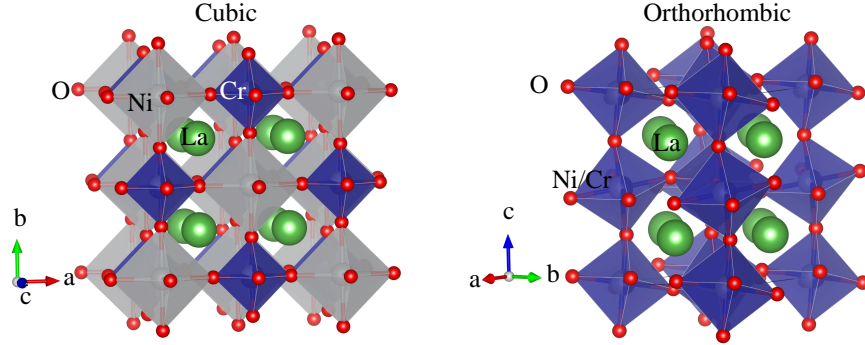


Figure 1: The ordered cubic (left figure) and the disordered orthorhombic (right figure) octahedral structure of LCNO.

propose us to study the underlying physics in detail.

First principle density functional theory (DFT) [22] is the most dependable technique to study the energy bands and electronic structure of these strongly correlated electron systems. In DFT, the generalised gradient approximation (GGA) [23] along with the Coulomb potential  $U$  (GGA+ $U$ ) [24] method is widely accepted model to analyse the  $d$  and  $f$  electrons in strongly correlated systems. But this model is only studied to know the ground state properties of these materials. The Monte Carlo simulation technique has been used to study the thermally activated magnetic behaviour. There are several theoretical model such as 3d Ising model [25], Mean field theory [26], 3d Heisenberg model [27] etc, to explain this behaviour appropriately.

At this point, we have chosen one of double perovskite  $\text{La}_2\text{CrNiO}_6$  (LCNO), which may be a suitable candidate to spintronics application. LCNO is studied theoretically based on a computer generated lattice parameters, which is not actually right for this material [20]. So, we have revisited the complete theoretical studies with the real lattice parameters and space group

which is determined experimentally. The electronic structure and detailed optical properties have been studied with two different symmetry cubic and orthorhombic, calculated from the rietveld refinement [28]. After the detailed calculations, it is seen that disordered orthorhombic is more close to experimental values than the ordered cubic structure. The temperature dependent magnetic studies is very similar to the experimental one. We have then calculated the magnetocaloric effect of LCNO using the Monte Carlo simulation [29]. The calculated relative cooling power (RCP) is very attractive to use it as magnetocaloric material for magnetic cooling.

## 2. Experimental Details

The Sol-Gel technique was applied to synthesize the double perovskite  $\text{La}_2\text{CrNiO}_6$ . The metallic nitrates  $\text{La}(\text{NO}_3)_3 \cdot 6\text{H}_2\text{O}$ ,  $\text{Cr}(\text{NO}_3)_3 \cdot 9\text{H}_2\text{O}$  and  $\text{Ni}(\text{NO}_3)_2 \cdot 6\text{H}_2\text{O}$  were taken with appropriate stoichiometric ratio and mixed in magnetic stirrer for 1 hour with the de-ionised water medium. Then the citric acid and ethylene glycol were taken with appropriate molar ratio to the solution where they were used as a fuelling and stabilizing agent respectively. The whole solution was stirred 5 hours and then heated around 473 K to form the gel and further heating caused a auto-combustion to achieve fluffy precursor LCNO powder. The obtained powder was then grinded and calcined at 1173 K and then it was pelletized with binding element polyvinyl chloride. Atlast, the sample was sintered at 1223 K to achieve the final LCNO powder. The room temperature X-ray diffraction (XRD) pattern of LCNO was obtained in X-ray powder diffractometer (Rigaku Miniflex II, Cu-K $\alpha$  :  $\lambda=1.54 \text{ \AA}$ ), where the range of  $2\theta$  is  $10^\circ$  to  $80^\circ$  at a scanning rate of  $0.02^\circ$  per step. The

crystal structure and the lattice parameters were extracted from the Rietveld refinement of the XRD data using the Fullprof suite program [30].

Table 1: Atomic coordinates and lattice parameters of LCNO. The Muffin-Tin radii (RMT) of all atom used in WIEN2k described the right column of this table.

Symmetry	Atom	x	y	z	lattice parameters	RMT (Å)
Cubic	La	0.2500	0.2500	0.2500	a = 7.7562	2.50
Fm-3m	Ni	0.5000	0.5000	0.5000		2.02
( $\chi^2=1.26$ )	Cr	0.5000	0.5000	0.5000		1.85
	O	0.0000	0.3366	0.0000		1.67
Orthorhombic	La	0.4980	0.0164	0.2500	a = 5.5008	2.47
Pbnm	Ni	0.0000	0.0000	0.0000	b = 5.4654	1.86
( $\chi^2=1.24$ )	Cr	0.0000	0.0000	0.0000	c = 7.7583	1.82
	O1	0.5555	0.4987	0.2500		1.60
	O2	0.2131	0.2530	0.0441		1.60

### 3. Computational Details

#### 3.1. *Ab-initio* Calculations

The electronic structure and the magnetic properties of LCNO is being studied using the first principle density functional theory. The full-potential linearized augmented plane wave (FPLAPW) method have been implemented to solve the Kohn-Sham equations as described in WIEN2K package [31, 32]. The crystal structure optimization and the electronic properties as well as the magnetic moments of each ions have been calculated using the

spin polarized general gradient approximation (GGA) with Coulomb repulsion  $U$  (GGA+ $U$ ) method. As the LCNO has shown two symmetric structures (discuss later) cubic and orthorhombic, the electronic and magnetic properties have been studied according to these symmetries. The muffin-tin radii ( $R_{mt}$ ) for La, Cr, Ni and O atoms are 2.26 Å, 1.89 Å, 1.78 Å and 1.69 Å for cubic respectively. For orthorhombic these radii are 2.26 Å, 1.89 Å, 1.78 Å and 1.69 Å respectively. The cut-off energy ( $R_{mt} \times K_{max}$ ) from core states to valance states has been set to 6 and 7 eV respectively.  $17 \times 17 \times 17$  k-points have been adopted in the whole Brillion zone for self-consistent convergence for cubic phase and  $10 \times 10 \times 8$  for orthorhombic one. The Hubbard parameter  $U_{eff} = U - J = 4$  eV and 6 eV have been used for Cr-d and Ni-d orbitals respectively. The energy and charge convergence criteria have been fixed to  $10^{-4}$  Ry and  $10^{-3}$  e respectively for self-consistent optimize calculations of LCNO. In order to stabilize the crystal structures for both the cases, the structural optimization have done to find the optimize lattice parameter. After that the different magnetic spin configuration was adopted such as, ferromagnetic (FM) and three type of antiferromagnetic (AFM) (A-AFM, C-AFM, G-AFM). Among them the ferromagnetic configuration has the minimum energy for both the symmetries. The magnetic moment of the individual atoms are then calculated and they are discuss in detail in the following section. The detail optical properties of LCNO for both structures have been analyzed of the optimize crystal structure.

The frequency dependent dielectric function  $\varepsilon(\omega)$  has been investigated to study the optical properties. It can be expressed as  $\varepsilon(\omega) = \varepsilon_1(\omega) + j\varepsilon_2(\omega)$ , where  $\varepsilon_1(\omega)$  and  $\varepsilon_2(\omega)$  signify the real and imaginary component of the com-

plex dielectric function  $\varepsilon(\omega)$ .  $\varepsilon_2(\omega)$  is determined from the following equation.

$$\varepsilon_2(\omega) = \frac{2e^2\pi}{\Omega\varepsilon_0} \sum_{k,v,c} (|\psi_k^c| \mathbf{u} \cdot \mathbf{r} |\psi_k^v|)^2 \delta(E_k^c - E_k^v - E) \quad (1)$$

Where  $(|\psi_k^c| \mathbf{u} \cdot \mathbf{r} |\psi_k^v|)^2$  represents the matrix elements for the direct transfer from the valance state to conduction state,  $E_k^c - E_k^v$  is the excitation energy and  $\psi_k^v$  and  $\psi_k^c$  are the Bloch wave-functions for the valance and conduction band with the wave-vector  $k$ . The real component of the dielectric function is derived from the imaginary part  $\varepsilon_2(\omega)$  by using Kramers-Kronig relation,

$$\varepsilon_2(\omega) = 1 + \frac{2}{\pi} P \int_0^\infty \frac{\omega' \varepsilon_2(\omega')}{\omega'^2 - \omega^2} d\omega' \quad (2)$$

where  $P$  is the principle value of the integral. Using the value of the dielectric functions, we have calculated other optical properties such as reflectivity ( $R(\omega)$ ), refractive index ( $n(\omega)$ ), absorption coefficient ( $\alpha(\omega)$ ) and optical conductivity ( $\sigma(\omega)$ ). These parameters are determined from the following equations respectively.

$$R(\omega) = \left| \frac{\sqrt{\varepsilon(\omega)} - 1}{\sqrt{\varepsilon(\omega)} + 1} \right|^2 \quad (3)$$

$$n(\omega) = \frac{1}{\sqrt{2}} (\sqrt{\varepsilon_1(\omega)^2 + \varepsilon_2(\omega)^2} + \varepsilon_1(\omega))^{\frac{1}{2}} \quad (4)$$

$$\alpha(\omega) = \sqrt{2}\omega (\sqrt{\varepsilon_1(\omega)^2 + \varepsilon_2(\omega)^2} - \varepsilon_1(\omega))^{\frac{1}{2}} \quad (5)$$

$$\sigma(\omega) = -\frac{j\omega}{4\pi} \varepsilon(\omega) \quad (6)$$

All of these parameters are calculated with a mesh of 1000  $k$  points over the irreducible Brillouin zone.

### 3.2. Monte Carlo Simulations

The strongly correlated system has the strong anisotropy in spin configuration. For that reason we have chosen the anisotropic Heisenberg spin model to do the Monte Carlo simulations. But For LCNO, the model has failed to satisfy the experimental data at low temperatures. So that we have tried with the discrete Ising spin model for the simulations and it satisfactorily agreed with the experimental study. Actually, for LCNO there is two type magnetic ions; the spin values ( $S$ ) of both ions,  $\text{Cr}^{3+}$  as well as  $\text{Ni}^{3+}$  are  $3/2$ . So that the anisotropy in the spin configuration vanishes itself due to double perovskite structure, which bounds themselves to keep the same number of loan electrons in their 3d orbitals. However, we have taken the Ising model Hamiltonian for the simulation.

$$H = -J \sum_{\langle i,j \rangle} s_i s_j - h \sum_i s_i \quad (7)$$

Where  $J$  and  $h$  is interaction constant and applied field respectively. From previous experimental study of LCNO, we have seen that the ordering temperature is  $T_C = 110$  K. In our magnetic Monte Carlo simulation study, we have considered the magnetic  $\text{Cr}^{3+}$  ion and  $\text{Ni}^{3+}$  ion are randomly situated at the corner of the cubic crystal structure and the interactions between two magnetic ions have chosen to ferromagnetic. We have used the mean field approximation [33] to determine the interaction constant  $J$ .

$$T_N = \frac{2}{3k_B} Z S(S+1) J \quad (8)$$

The value of the transition temperatures ( $T_N = 110$  K) are taken from the previous experimental study and  $Z$  are the co-ordination number (Here  $Z =$

6 and  $S = 3/2$ ). The values of  $J$ , which have been calculated from equation (2), are 7.46 K.

We have performed the Monte Carlo simulation (MCS) using the single flip Metropolis algorithm to calculate the magnetic properties of LCNO. The periodic boundary condition and standard sampling method have been implemented to the whole lattice of size  $L = 30$  in all three Cartesian directions. If the change in energy ( $dE$ ) is less than zero, or the transition probability [ $\exp(-dE/k_B T)$ ] is greater than a random value, the flip is accepted otherwise rejected.  $10^6$  MCS steps have been used to reach the equilibrium of lattices and next  $10^7$  steps to average the magnetization and other observables. The physical quantities, which have been measured using MCS, are described as follows [34]. The internal energy per site is,

$$E = \frac{1}{N} \langle H \rangle \quad (9)$$

Where  $N = L \times L \times L$  is the total number of lattice points. The magnetisation of LCNO is,

$$M = \langle \frac{1}{N} \sum_i S_i \rangle \quad (10)$$

The magnetic susceptibility is given by,

$$\chi = \frac{\langle M^2 \rangle - \langle M \rangle^2}{k_B T} \quad (11)$$

The magnetic specific heat is calculated by,

$$C_m = \frac{\langle E^2 \rangle - \langle E \rangle^2}{k_B T^2} \quad (12)$$

The magnetic entropy is given by

$$S_m = \int_0^T \frac{C_m}{T} dT \quad (13)$$

The change in magnetic entropy is described as

$$\Delta S_m = \int_0^{h_{max}} \left( \frac{\partial M}{\partial T} \right) dh \quad (14)$$

Where  $h_{max}$  is the maximum applied field and  $\left( \frac{\partial M}{\partial T} \right)_h$  is the thermal magnetisation for a fixed external magnetic field  $h$ . The adiabatic temperature change is given by

$$\Delta T_{ad} = -T \frac{\Delta S_m}{C_m} \quad (15)$$

The magnetocaloric effect is measured by a parameter called Relative Cooling Power (RCP), which is calculated from the magnetic entropy change vs temperature curves. The formula for determining of RCP is given by,

$$RCP = \int_{T_1}^{T_2} \Delta S_m(T) dT \quad (16)$$

Where,  $T_1$  and  $T_2$  are the cold and hot temperature corresponding the both ends of half maximum value of  $\Delta S_m$  vs  $T$  curves.

## 4. Results and Discussions

### 4.1. Crystallographic Information

The Rietveld refinement of the XRD data is being performed to determine the crystal structure of LCNO. In this context, we have tried to fit the experimental data with orthorhombic Pbnm space group as stated earlier [35]. The pseudo-voigt function is being imposed to match the peaks where as the base is fitted with the fifth order polynomial function as described in Fullprof software. A parameter which defines the good correlation with the experimental and theoretical results called the goodness of fit ( $\chi^2$ ). The minimum value of  $\chi^2$  means a good refinement. In our case it is 1.24, which turns

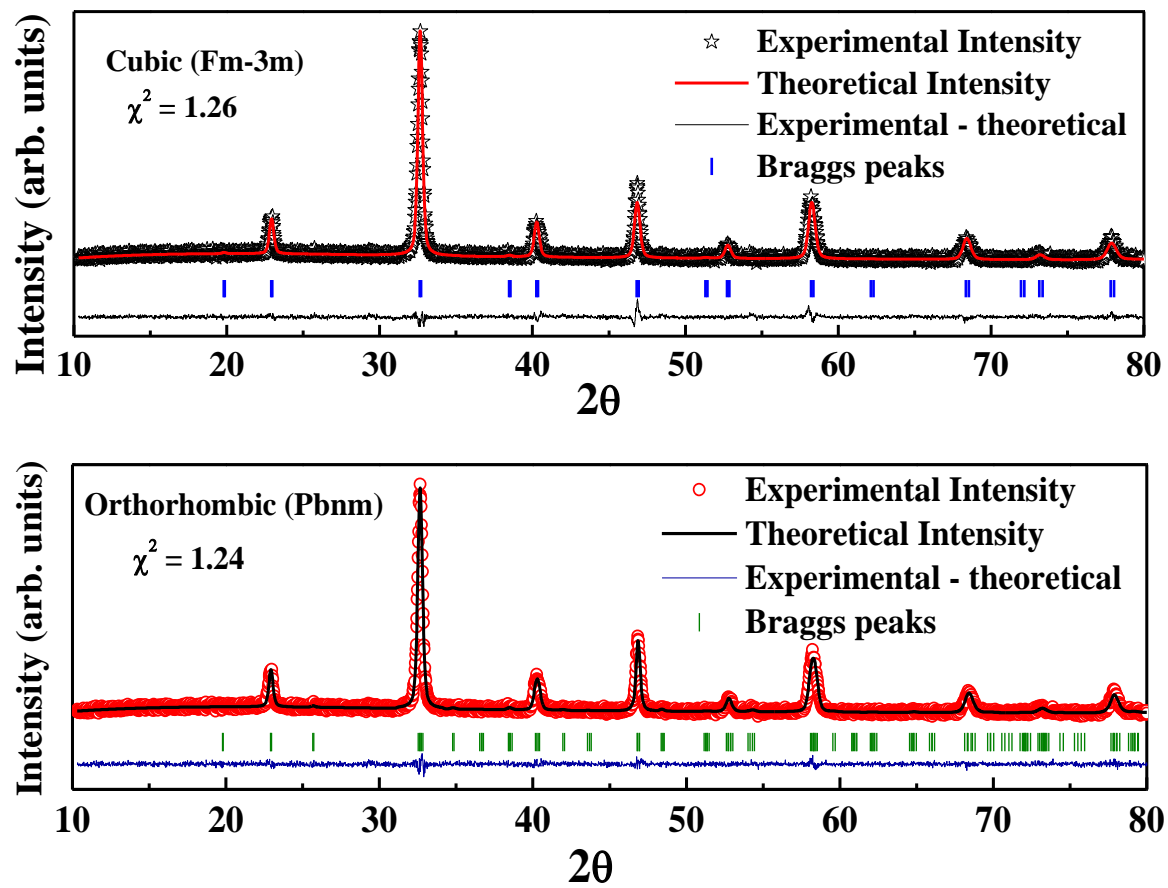


Figure 2: The rietveld refinement of the experimental XRD data of cubic (upper) and orthorhombic (lower) LCNO. The description of colours have shown in figures.

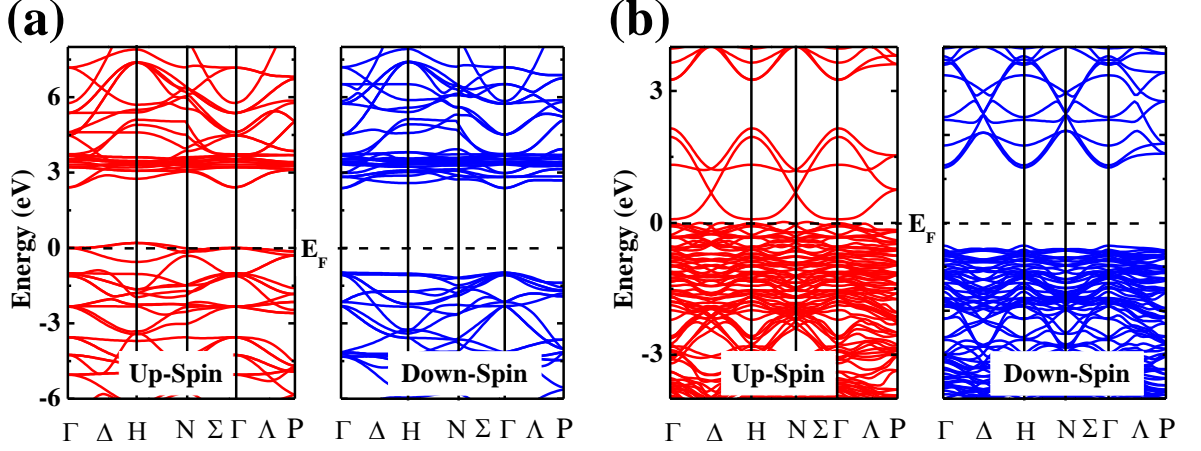


Figure 3: The band structure plot of LCNO (a) cubic (b) orthorhombic. The Fermi energy ( $E_F$ ) is set to zero, shown with the horizontal dotted line.

out the difference curve with experimental and theoretical intensities to a straight line in figure 2(b).

The stability of LCNO double perovskite may be now approximated using the La-O, Ni-O, Cr-O bond lengths from the above refined data. It can be analysed by Goldschmidt's tolerance factor [36], stated as

$$t = \frac{R_{La} + R_O}{\sqrt{2}(\frac{R_{Cr} + R_{Ni}}{2} + R_O)} \quad (17)$$

Where the  $R_{La}$ ,  $R_{Ni}$ ,  $R_{Cr}$ ,  $R_O$  are the ionic radii of La, Ni, Cr, O atoms, respectively. The ionic radii of these atoms are 1.16 Å, 0.69 Å, 0.61 Å and 1.4 Å respectively and the value of tolerance factor turns out to 0.89, which is the limiting value of orthorhombic phase. According to the Goldschmidt's, the value of tolerance factor should be 0.75 to 0.9 for orthorhombic and 0.9 to 1 for cubic phase. So this tolerance value motivates us to further refinement of LCNO with cubic Fm-3m symmetry. In figure 1(a), we have shown the

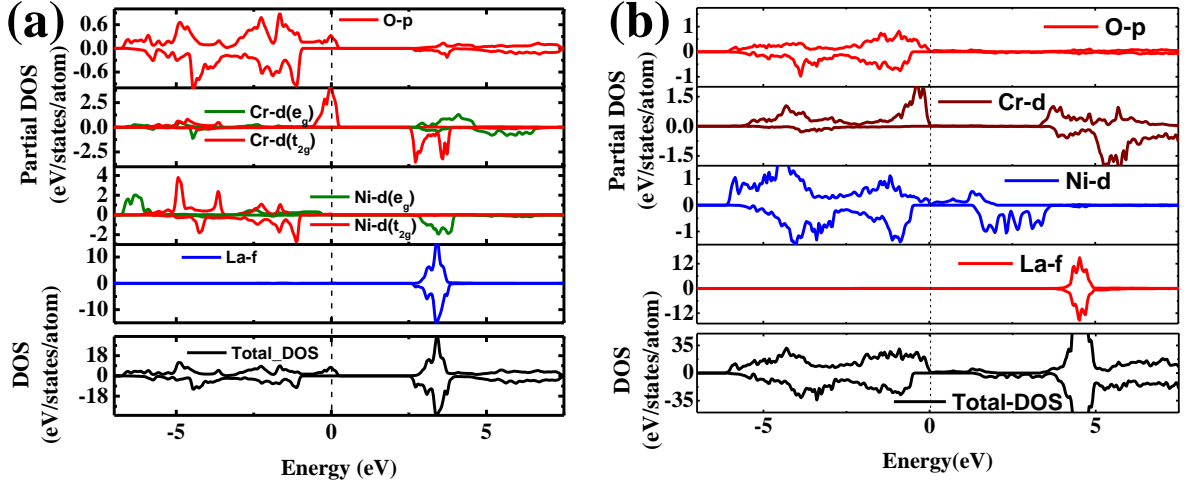


Figure 4: The total and partial density of states of LCNO for (a) cubic and (b) orthorhombic structures.

XRD fitting with cubic phases and it also turns out to a nice correlation with the experimental intensities. According to the  $P6mm$  space group the B-site cations are disordered and form a randomly oriented B and B' sublattices. In the orthorhombic crystal structure, the Cr and Ni belong to the same 4a Wyckoff site. Whereas for cubic structure, these atoms have 4b and 4a sites respectively. The lattice parameters and the atomic positions of both the symmetry group have been described in table 1. Which one is more preferable by nature between these symmetries is being discussed using the DFT calculations in the following sections.

#### 4.2. Spin-polarized electronic structure

The spin polarized electronic band structure plays a very important role to explain the most of the physical properties of materials. The optical properties and charge transport mechanism largely depend on the energy

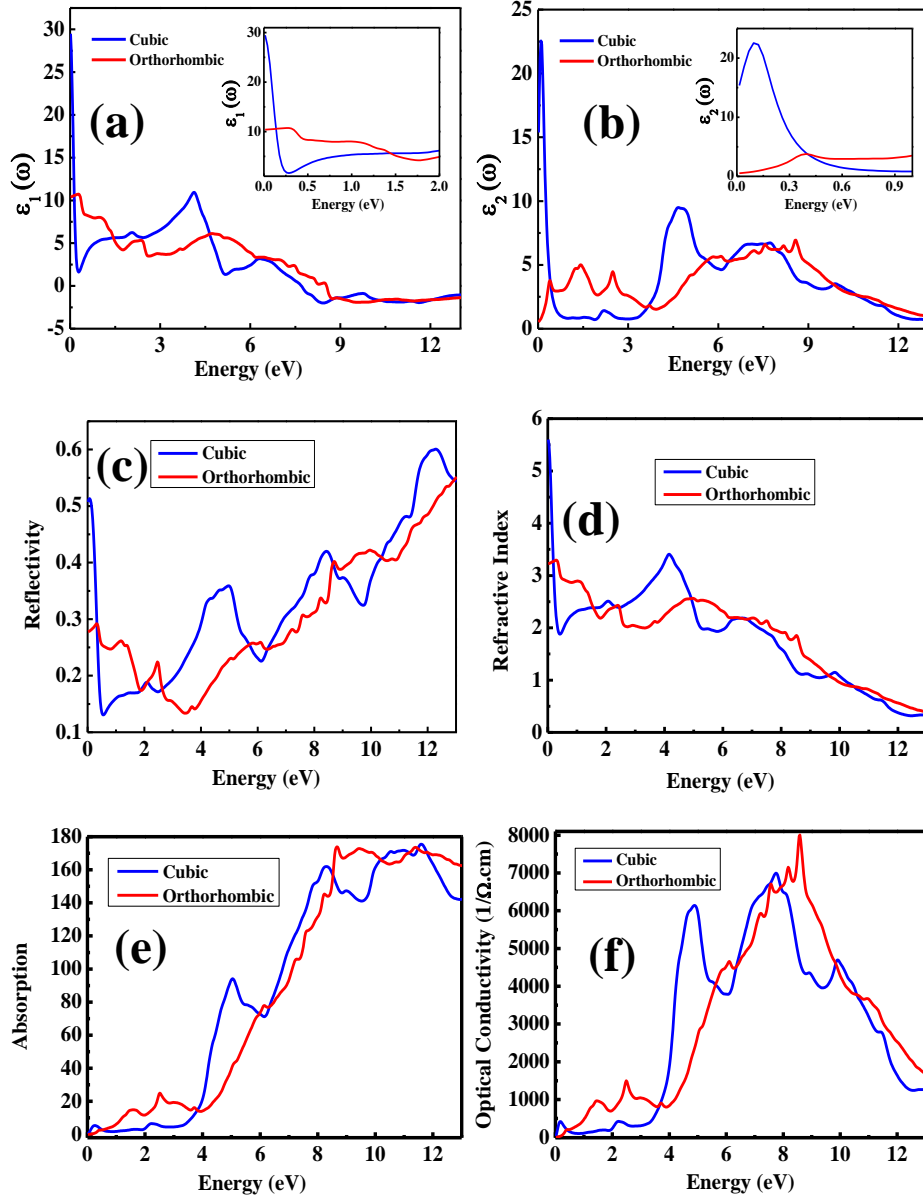


Figure 5: (upper-left) The real part and (upper-right) imaginary part of the complex optical dielectric function, inset of both the figure are the larger view in the lower energy. The reflectivity (middle-left), refractive index (middle-right), absorption (lower-left) and optical conductivity (lower-right) of LCNO. Blue and red colour plots are described for the cubic and orthorhombic structure respectively.

band gap of the semiconductors. After optimizing the experimental lattice parameters and positions, the ground state band structure is calculated using GGA+U method along the high symmetry direction within the Brillouin zone. In the up-spin channel the band structure have shown a very little spike above the Fermi energy at H- point in figure 3(a). So, the valance band maxima (VBM) crosses the limit of the Fermi energy ( $E_F$ ), which means the cubic Fm-3m structure possesses a metallic character in the ground state. In the minority spin channel, the value of the energy band gap is 3.4 eV. The VBM and CBM (conduction band minima) are in the same  $\Gamma$  point, which indicates the direct band gap presents in this material. Figure 3(b) represents the band structure of LCNO for orthorhombic Pbnm space group. Here one of the conduction energy band is very close to the Fermi energy in the majority spin channel. The band gap between VBM and CBM is 0.08 eV, which is negligibly small as like the silver selenide ( $\text{Ag}_2\text{Se}$ ) [37]. So, the orthorhombic LCNO belongs to a narrow band gap semiconductor category in the up-spin channel. Again the down-spin channel has a wide direct band gap ( $\Gamma - \Gamma$ ) 1.9 eV. The detail study of the ground state electronic band structure justifies that LCNO belongs to a half- metallic perovskite family.

In order to understand the features of the band structures, the density of states (DOS) of all the atoms and the total DOS is studied in detail in this section. The DOS also predicts the nature of bonding as well as the electronic states of different energy levels. The partial and total DOS of all atoms have shown in figure 4 for both the structures. Here the Fermi energy is set to zero electron volt. The left and right side of it corresponds valance electrons state and conduction electrons state respectively. The positive and

negative values of the states along the Y-axis signify the spin-up and spin-down channel respectively. The valance band mainly consists of the Cr-3d and Ni-3d orbitals hybridized with the O-2p orbital for both the structures. Similarly the conduction band is dominated by La-4f state and the 3d states of Cr and Ni atoms. The PDOS of La-f, which is symmetric with respect to the spin up and down channel, signifies that it is non magnetic in nature. For cubic structure in the up-spin channel, the PDOS of Cr clearly shows that Cr-d state (precisely Cr-d( $t_{2g}$ )) runs over the Fermi level. In the octahedral arrangement the  $t_{2g}$  orbital is occupied, which confirms the half metallic behaviour of LCNO. The asymmetric DOS of Cr and Ni also support the ferromagnetic spin alignment of these atoms, which will be discussed in detail in the next section. The PDOS of Ni shows that there is no states near the Fermi level. In the orthorhombic structure, it is clearly seen that the Cr-d state is bellow the Fermi energy so the total DOS. But the Ni-d states is very close to the Fermi level. The maxima of the conduction states is shifted towards the higher energy from cubic to orthorhombic symmetry. The hybridization between La-4f and O-2p is very weak than the Cr-3d and O-2p, Ni-3d and O-2p. This corresponds the La-O bond is ionic type whereas the Cr-O and Ni-O have strong covalent bond.

#### *4.3. Optical properties*

The investigation of the optical properties is very important for a material, which may be used in the opto-electronic device applications. Though the energy dependent optical parameters, which are mainly influenced by the energy band structures, inform us about the occupied and unoccupied states related to the energy bands. So, the real ( $\varepsilon_1(\omega)$ ) and imaginary ( $\varepsilon_2(\omega)$ )

part of the dielectric function have been determined from the equation (1) and (2). Now, all the other optical and absorptive properties such as reflectivity, refractive index, absorption coefficient and optical conductivity have been calculated from the dielectric functions  $\varepsilon_1(\omega)$ ,  $\varepsilon_2(\omega)$  and  $\varepsilon(\omega)$ . For cubic and orthorhombic symmetries, all the optical parameters with respect to the energy are described in fig.5(a-f) with blue and red colour respectively. For cubic structure, we have seen only one non zero component,  $\varepsilon^{xx}(\omega) = \varepsilon^{yy}(\omega) = \varepsilon^{zz}(\omega)$  of the second order dielectric tensor. But in orthorhombic case, the tensor has three different non zero component along three axis. For simplification in the comparison between two structures, we have taken the average  $[(\varepsilon^{xx}(\omega) + \varepsilon^{yy}(\omega) + \varepsilon^{zz}(\omega))/3 = \varepsilon^{avg}(\omega)]$  of these components and plotted in the fig.5.

The real (dispersive) and imaginary (absorptive) components as the function of photon energy are plotted in fig.5(a) and (b) respectively. The absorptive component  $\varepsilon_2(\omega)$  describes the optical transition mechanism between the energy bands in the materials. The transition between the highest occupied orbitals in the valance band and minimum unoccupied orbitals in conduction band produces the optical spectra in the materials. According to the selection rules the allowed optical transitions are  $s \rightarrow p$ ,  $p \rightarrow d$ ,  $d \rightarrow p$ ,  $d \rightarrow f$  etc.,. The first optical transitions at 0.15 eV and 0.4 eV for cubic and orthorhombic structures respectively [inset of fig.5(b)]. The values are significantly low, which justify the narrow band gap of LCNO. Beyond the threshold, there are four significant transitions for orthorhombic at 1.5 eV, 2.5 eV, 6 eV and 9 eV. These transitions mainly from the O-2p orbital (VB) to Ni-3d, Cr-3d, La-5d (CB) and Ni-3d, Cr-3d to La-4f orbital. Similarly for the cubic structures,

there are three main transition at 2.25 eV, 5 eV and 7.5 eV apart from the threshold one. The dispersive part  $\varepsilon_1(\omega)$  of dielectric function shows that it starts a maximum value at  $\varepsilon_1(0)$  and then creates some peaks and ends in the negative value for both the structures. The negative value of  $\varepsilon_1(\omega)$  indicates that the incident electromagnetic radiation is totally reflected from this medium in this energy range, which corresponds the presence of the metallic character in LCNO. So, this material can be used as a electromagnetic radiation protective purposes. The value of  $\varepsilon_1(\omega)$  at zero energy ( $\omega = 0$ ) is known as optical dielectric constant. For the cubic and orthorhombic symmetries, the values of  $\varepsilon_1(0)$  are 30 and 10 respectively.

Fig.5(c) represents the reflectivity spectra in the photon energy range 0 eV to 13 eV for both the structures. The reflectivity is about to 50% at 0 eV for cubic symmetry and decreases sharply to minimum value at 0.5 eV, after that it varies from 15% to 50% upto 11 eV and reaches a maximum 60% at 12 eV. Where as the orthorhombic structure, the reflectivity goes to a minimum at 3.5 eV and reaches the maximum 55% in this energy range. The refractive index  $n(\omega)$  is a very important parameter for determining the amount of light bent or refracted by the material. From fig.5(d), it is seen that the near  $\omega = 0$  the  $n(\omega)$  has a large value and decreases sharply in 0 eV to 0.5 eV energy range due to the metallic nature in cubic symmetry. The  $n(\omega)$  has reached a maximum value of 3.5 at 4 eV and decreased towards zero with increasing photon energy. But the orthorhombic symmetry, the static refractive index were determined 3.2, calculated at 0 eV. Above 10 eV the value of  $n(\omega)$  became less than the unity. This is called the superluminal phenomenon where the speed of light in the material goes beyond the vacuum.

This effect may be useful in the optical networks, optical communications and optoelectronic applications.

The excitation energy of a electron for passing the band gap of the material directly depends on the absorption of photons of light. The amount of power absorbed when the light is passing through a unit thickness of solid is called the absorption coefficient  $\alpha(\omega)$ . This  $\alpha(\omega)$  is directly related to the imaginary component of dielectric function  $\varepsilon_2(\omega)$ . In case of cubic symmetry (fig.5(e)), the absorption function has peaks at 2.2 eV, 5 eV and 8 eV, which correspond the inter-band transitions and the  $\alpha(\omega)$  gradually takes the higher values with the high energy transitions. For orthorhombic structure it has peaks at 1.5 eV, 2.5 eV and 6 eV, which are as same as the  $\varepsilon_2(\omega)$ . The optical conductivity  $\sigma(\omega)$  is described in fig.5(f), which shows three significant peaks for cubic structures. The orthorhombic symmetry of LCNO has two low energy peaks (1.6 eV and 2.2 eV), which correspond the electron transition in the visible range of the spectra. After reaching a maximum value, the  $\sigma(\omega)$  decreases in the high energy (above 10 eV) for both cubic and orthorhombic structures of LCNO.

Table 2: Calculated magnetic moments of each atoms, interstitial and cell for LCNO in  $\mu_B$  unit

Symmetry	$\mu_{La}$	$\mu_{Ni}$	$\mu_{Cr}$	$\mu_O$	$\mu_{int}$	$\mu_{cell}$
Cubic	0.01	1.69	1.96	0.009	0.26	3.99
Orthorhombic	0.01	1.07	2.53	-0.001	1.50	16.00

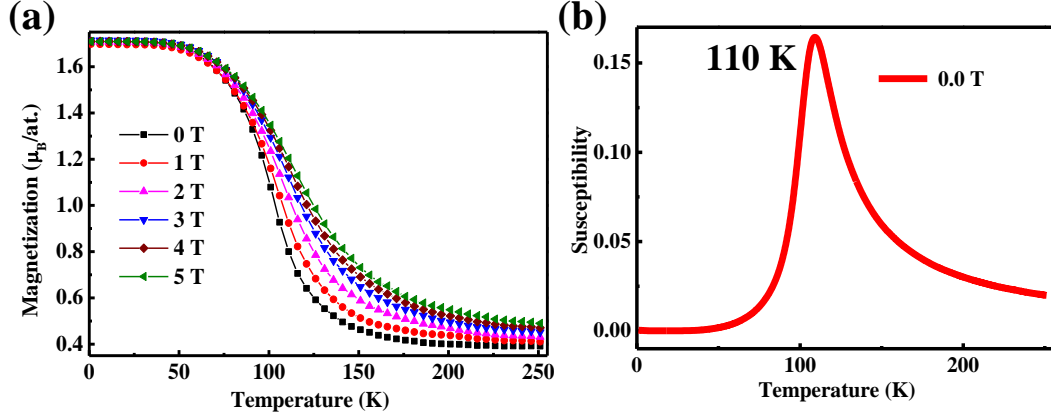


Figure 6: (a) Magnetization vs temperature plot at different applied field. (b) Magnetic susceptibility plot at zero applied field.

#### 4.4. Magnetic properties

The magnetic properties of LCNO turns out to be an interesting one due to the interaction between the two magnetic atoms Cr and Ni through the oxygen with octahedral arrangement in the perovskite structure. To study the magnetic properties in detail, the stable ground state magnetic structure is determined through the energy minimization of different magnetic structures for both the cases (cubic and orthorhombic). The ferromagnetic (FM) configuration has the lower energy value than the other three anti-ferromagnetic (AFM) spin orientations G-AFM, C-AFM and A-AFM. The magnetic moments of the individual atoms and the interstitial of cubic and orthorhombic structures of LCNO are calculated using the DFT. The moments are described in table 2 for both the structures. In the orthorhombic structures, the magnetic moment of Ni and Cr are  $1.07 \mu_B$  and  $2.53 \mu_B$  respectively. The spin only moment is  $3.87 \mu_B$  for both  $\text{Ni}^{3+}$  as well as  $\text{Cr}^{3+}$

ions. It is calculated from this formula stated as,  $\mu = \sqrt{n(n+2)}$  (where  $n$  = number of unpair electrons in d-orbital). The experimental effective magnetic moment of LCNO, reported by Palakkal et al. is  $4.01 \mu_B/\text{f.u}$  [35]. The total magnetic moment in a cell of LCNO is obtained  $16.00 \mu_B$  (see Table 2). The magnetic moment per magnetic ion for our case becomes  $4.00 \mu_B$  (there are four magnetic ion in the whole cell), which is exactly same as the experimental data Palakkal et al. [35]. The obtained magnetic moment of  $\text{Ni}^{3+}$  is significantly less than formulated value. In the octahedral arrangement of LCNO, the crystal field effect causes the 3d orbital splitting ( $e_g$  and  $t_{2g}$ ) of Ni and Cr atom. Due to the stronger ligand field, the splitting energy ( $\Delta$ ) of  $\text{Ni}^{3+}$  becomes large enough to be a low spin state. So, the number of unpair electron in the 3d orbital turns out to one. Goodenough et al showed that in  $\text{LaNi}_{0.5}\text{Mn}_{0.5}\text{O}_3$  perovskite, the spin only moment of low spin  $\text{Ni}^{3+}$  has a value of  $1 \mu_B$ , which is matched with our calculated result [38]. The reduction of the magnetic moment of  $\text{Cr}^{3+}$  ion is due to the hybridization of 3d electrons with the O-2p states. The ordered cubic structure, the moment of Ni ( $1.6 \mu_B$ ) is slightly greater whereas, Cr has lesser moment of  $1.9 \mu_B$ . This happens because of the double exchange (DE) interaction, where one electron moves from O-2p orbital to the one unoccupied Ni- $e_g$  orbital and one Cr- $t_{2g}$  electron fills the gap in O-2p orbital. The DE interaction is mainly responsible for long- range FM ordering in LCNO.

Now, the temperature and field dependent magnetization and the phase transition are studied thoroughly using the monte carlo simulation under the metropolis algorithm [39]. Figure 6(a) represents the magnetization as a function of temperature at different magnetic field. Upon cooling, the value

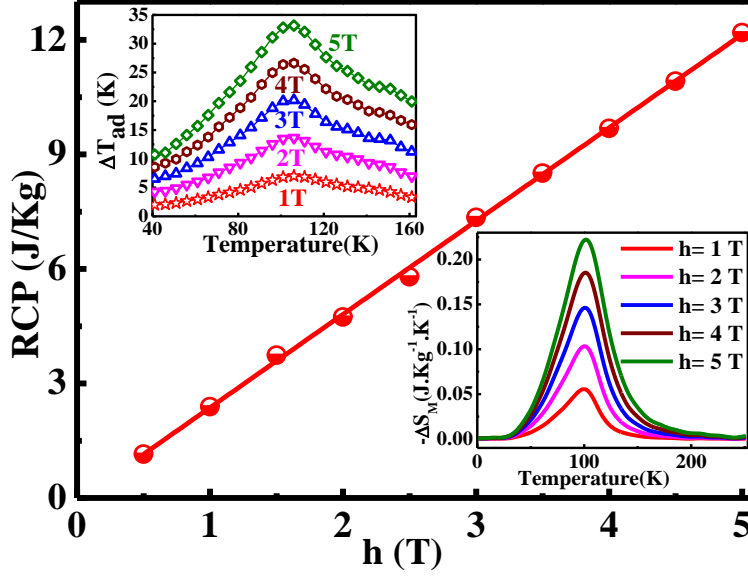


Figure 7: The RCP at different field, which varies linearly upto 5 T magnetic field. (upper-inset) Adiabatic temperature change with respect to the temperature at different magnetic field, (lower-inset) The isothermal entropy change at different applied field.

of the magnetization suddenly increases and reaches a maximum  $1.7 \mu_B/at$ . This type of behaviour is called the ferromagnetic phase transition. To determine the exact transition temperature ( $T_C$ ), the magnetic susceptibility ( $\chi$ ) is plotted in fig.6(b). The peak in the susceptibility curve at 110 K suggested the  $T_C$  of LCNO. The steepness of the curve gradually decreases with the applied field. The alignment of the spin increases with applied field in the paramagnetic region causes the increment of magnetization.

#### 4.5. Magnetocaloric effect

The magnetocaloric effect (MCE) is nothing but the heating as well as cooling of the magnetic materials under the application of external magnetic field. The range of heating or cooling defines the effectiveness of the mag-

netic materials. The MCE is characterized by the entropy change ( $\Delta S$ ) and the temperature change ( $\Delta T$ ) during the isothermal and adiabatic processes respectively. The adiabatic temperature change ( $\Delta T_{ad}$ ) with respect to the temperature at different magnetic field is shown in the upper inset of fig.7. The maximum change is recorded at the transition temperature and value of the maxima increases with higher magnetic field. The FWHM value of this curve describes the amount of cooling in the materials. The value of  $\Delta T_{ad}^{max}$  is 33 K with 5 Tesla applied field. The negative magnetic entropy change  $\Delta S_M$  is shown in the lower inset of fig.7. It is negative in the entire temperature range. The peak value gradually increases from 0.05 J/Kg.K to 0.24 J/Kg.K with applied field change from 1 Tesla to 5 Tesla. The operating temperature range for cooling of the material determines from the FWHM of the  $\Delta S_M$  versus T (K) curve. For this purpose the RCP is calculated at different applied field and it is proportional to the field. The RCP value is 12 J/Kg at 5 T, which is good for magnetocaloric applications.

## 5. Conclusions

We have studied the electronic, optical and magnetic properties of LCNO using the first principle DFT calculations and reinvestigated the magnetic properties and magnetocaloric effect using the monte carlo simulation method. Some theoretical studies have reported earlier without the experimental evidence on the basis of unrealistic structures. But, we have done all the calculations from the experimental xrd structure and the obtained results have followed the experimental one. From the xrd refinement, we have seen that there are two symmetries (orthorhombic- Pbnm and cubic- Fm-3m), which

have fitted nicely with the experimental one. According to these structures, we have investigated these properties and compared with the experiment. From the band structures and DOS of the both structures, we have concluded that LCNO has the half metallic properties and magnetic properties confirm that it is ferromagnetic also. It has high dielectric constant and refractive index. All these properties suggest that it is a very good candidate for spintronic applications. We have conclude that the orthorhombic Pbnm space group is more experimentally accepted than the cubic one. Needless to say, the magnetocaloric study also shows that it has a good RCP value for magnetic refrigeration.

## References

- [1] D. Serrate, J. M. D. Teresa, M. R. Ibarra, Double perovskites with ferromagnetism above room temperature, *Journal of Physics: Condensed Matter* 19 (2006) 023201.
- [2] Y. Moritomo, T. Akimoto, A. Nakamura, K. Ohoyama, M. Ohashi, Antiferromagnetic metallic state in the heavily doped region of perovskite manganites, *Phys. Rev. B* 58 (1998) 5544–5549.
- [3] W. Prellier, V. Smolyaninova, A. Biswas, C. Galley, R. L. Greene, K. Ramesha, J. Gopalakrishnan, Properties of the ferrimagnetic double perovskites  $A_2FeReO_6$  ( $A = Ba$  and  $Ca$ ), *Journal of Physics: Condensed Matter* 12 (2000) 965–973.
- [4] S. Halder, M. Sheikh, B. Ghosh, T. Sinha, Electronic structure and electrical conduction by polaron hopping mechanism in  $A_2LuTaO_6$  ( $A=$

- Ba, Sr, Ca) double perovskite oxides, *Ceramics International* 43 (2017) 11097 – 11108.
- [5] H. Das, U. V. Waghmare, T. Saha-Dasgupta, D. D. Sarma, Electronic structure, phonons, and dielectric anomaly in ferromagnetic insulating double perovskite  $\text{La}_2\text{NiMnO}_6$ , *Phys. Rev. Lett.* 100 (2008) 186402.
- [6] S. Baidya, T. Saha-Dasgupta, Electronic structure and phonons in  $\text{La}_2\text{CoMnO}_6$ : A ferromagnetic insulator driven by coulomb-assisted spin-orbit coupling, *Phys. Rev. B* 84 (2011) 035131.
- [7] B. Kim, J. Lee, B. H. Kim, H. C. Choi, K. Kim, J.-S. Kang, B. I. Min, Electronic structures and magnetic properties of a ferromagnetic insulator:  $\text{La}_2\text{MnNiO}_6$ , *Journal of Applied Physics* 105 (2009) 07E515.
- [8] W. Yi, Y. Matsushita, A. Sato, K. Kosuda, M. Yoshitake, A. A. Belik,  $\text{Bi}_3\text{Cr}_{2.91}\text{O}_{11}$ : A ferromagnetic insulator from  $\text{Cr}^{4+}/\text{Cr}^{5+}$  mixing, *Inorganic Chemistry* 53 (2014) 8362–8366. PMID: 25089932.
- [9] H. Lin, X. X. Shi, X. M. Chen,  $\text{LaRNiMnO}_6$  (R = Pr, Nd, Sm) double perovskites with magnetodielectric effects, *Journal of Alloys and Compounds* 709 (2017) 772 – 778.
- [10] N. Rogado, J. Li, A. Sleight, M. Subramanian, Magnetocapacitance and magnetoresistance near room temperature in a ferromagnetic semiconductor:  $\text{La}_2\text{NiMnO}_6$ , *Advanced Materials* 17 (2005) 2225 – 2227.
- [11] J. Yang, J. Kim, Y. Woo, C. Kim, B. Lee, Magnetoresistance in double perovskites  $\text{Ba}_{2-x}\text{La}_x\text{FeMoO}_6$ , *Journal of Magnetism and Magnetic*

Materials 310 (2007) e664 – e665. Proceedings of the 17th International Conference on Magnetism.

- [12] J. Y. Moon, M. K. Kim, Y. J. Choi, N. Lee, Giant anisotropic magnetocaloric effect in double-perovskite  $\text{Gd}_2\text{CoMnO}_6$  single crystals, Scientific Reports 7 (2017) 16099.
- [13] H.-Z. Lin, C.-Y. Hu, P.-H. Lee, A. Z.-Z. Yan, W.-F. Wu, Y.-F. Chen, Y.-K. Wang, Half-metallic property induced by double exchange interaction in the double perovskite  $\text{Bi}(\text{2})\text{BB}'\text{O}(\text{6})$  ( $\text{B}, \text{B}' = 3\text{d}$  Transitional Metal) via first-principles calculations, Materials (Basel, Switzerland) 12 (2019) 1844. 31174337[pmid].
- [14] H. Das, P. Sanyal, T. Saha-Dasgupta, D. D. Sarma, Origin of magnetism and trend in  $T_c$  in Cr-based double perovskites: Interplay of two driving mechanisms, Phys. Rev. B 83 (2011) 104418.
- [15] H. Nair, P. Ramachandran, S. Venkataraman, S. K, Exchange bias and memory effect in double perovskite  $\text{Sr}_2\text{FeCoO}_6$ , Applied Physics Letters 101 (2012) 142401.
- [16] J. Xu, C. Xu, J.-B. Liu, L. Bellaiche, H. Xiang, B.-X. Liu, B. Huang, Prediction of room-temperature half-metallicity in layered halide double perovskites, npj Computational Materials 5 (2019) 114.
- [17] S.-J. Chang, M.-H. Chung, M.-Y. Kao, S.-F. Lee, Y.-H. Yu, C.-C. Kaun, T. Nakamura, N. Sasabe, S.-J. Chu, Y.-C. Tseng,  $\text{GdFe}_{0.8}\text{Ni}_{0.2}\text{O}_3$ : A multiferroic material for low-power spintronic devices with high storage capacity, ACS Applied Materials & Interfaces 11 (2019) 31562–31572.

- [18] Y. Fu, H. Zhu, J. Chen, M. P. Hautzinger, X.-Y. Zhu, S. Jin, Metal halide perovskite nanostructures for optoelectronic applications and the study of physical properties, *Nature Reviews Materials* 4 (2019) 169–188.
- [19] Y.-M. You, W.-Q. Liao, D. Zhao, H.-Y. Ye, Y. Zhang, Q. Zhou, X. Niu, J. Wang, P.-F. Li, D.-W. Fu, Z. Wang, S. Gao, K. Yang, J.-M. Liu, J. Li, Y. Yan, R.-G. Xiong, An organic-inorganic perovskite ferroelectric with large piezoelectric response, *Science* 357 (2017) 306–309.
- [20] J. Wang, X. Hao, Y. Xu, Z. Li, N. Zu, Z. Wu, F. Gao, Cation ordering induced semiconductor to half metal transition in  $\text{La}_2\text{NiCrO}_6$ , *RSC Adv.* 5 (2015) 50913–50918.
- [21] A. K. Paul, M. Reehuis, V. Ksenofontov, B. Yan, A. Hoser, D. M. Többens, P. M. Abdala, P. Adler, M. Jansen, C. Felser, Lattice instability and competing spin structures in the double perovskite insulator  $\text{Sr}_2\text{FeOsO}_6$ , *Phys. Rev. Lett.* 111 (2013) 167205.
- [22] W. Kohn, L. J. Sham, Self-consistent equations including exchange and correlation effects, *Phys. Rev.* 140 (1965) A1133–A1138.
- [23] J. P. Perdew, K. Burke, M. Ernzerhof, Generalized gradient approximation made simple, *Phys. Rev. Lett.* 77 (1996) 3865–3868.
- [24] V. I. Anisimov, F. Aryasetiawan, A. I. Lichtenstein, First-principles calculations of the electronic structure and spectra of strongly correlated systems: the LDA+U method, *Journal of Physics: Condensed Matter* 9 (1997) 767–808.

- [25] A. L. Talapov, H. W. J. Blote, The magnetization of the 3D Ising model, *Journal of Physics A: Mathematical and General* 29 (1996) 5727–5733.
- [26] Toulouse, G., Gabay, M., Mean field theory for heisenberg spin glasses, *J. Physique Lett.* 42 (1981) 103–106.
- [27] C. Holm, W. Janke, Critical exponents of the classical three-dimensional heisenberg model: A single-cluster monte carlo study, *Physical Review B* 48 (1993) 936–950.
- [28] H. M. Rietveld, A profile refinement method for nuclear and magnetic structures, *Journal of Applied Crystallography* 2 (1969) 65–71.
- [29] K. Binder, D. Heermann, L. Roelofs, A. J. Mallinckrodt, S. McKay, Monte carlo simulation in statistical physics, *Computers in Physics* 7 (1993) 156–157.
- [30] J. Rodríguez-Carvajal, Recent advances in magnetic structure determination by neutron powder diffraction, *Physica B: Condensed Matter* 192 (1993) 55 – 69.
- [31] P. Blaha, K. Schwarz, P. Sorantin, S. Trickey, Full-potential, linearized augmented plane wave programs for crystalline systems, *Computer Physics Communications* 59 (1990) 399 – 415.
- [32] P. Blaha, K. Schwarz, F. Tran, R. Laskowski, G. K. H. Madsen, L. D. Marks, Wien2k: An apw+lo program for calculating the properties of solids, *The Journal of Chemical Physics* 152 (2020) 074101.

- [33] J. H. Van Vleck, On the theory of antiferromagnetism, *The Journal of Chemical Physics* 9 (1941) 85–90.
- [34] K. Binder, D. Heermann, *Monte Carlo Simulation in Statistical Physics : An Introduction*, volume 80, 2010.
- [35] J. P. Palakkal, T. Faske, M. Major, I. Radulov, P. Komissinskiy, L. Alff, Ferrimagnetism, exchange bias and spin-glass property of disordered  $\text{La}_2\text{CrNiO}_6$ , *Journal of Magnetism and Magnetic Materials* 508 (2020) 166873.
- [36] V. M. Goldschmidt, Die gesetze der krystallochemie, *Naturwissenschaften* 14 (1926) 477–485.
- [37] F. Kirchhoff, J. M. Holender, M. J. Gillan, Structure, dynamics, and electronic structure of liquid ag-se alloys investigated by ab initio simulation, *Phys. Rev. B* 54 (1996) 190–202.
- [38] A. Wold, R. J. Arnett, J. B. Goodenough, Some magnetic and crystallographic properties of the system  $\text{LaMn}_{(1-x)}\text{Ni}_x\text{O}_{3+\lambda}$ , *Journal of Applied Physics* 29 (1958) 387–389.
- [39] T. K. Bhowmik, T. P. Sinha, Al-dependent electronic and magnetic properties of  $\text{YCrO}_3$  with magnetocaloric application: An ab-initio and monte carlo approach, *Physica B: Condensed Matter* 606 (2021) 412659.